Numerical simulation of hypersonic boundary-layer instability using different gas models

By O. Marxen, G. Iaccarino AND E. S. G. Shaqfeh

1. Motivation and objectives

Prediction of heat load on the surface of vehicles (re-)entering a planetary atmosphere is important for heat-shield design. Turbulent flow induces a much higher heating in comparison to laminar flow. Therefore, prediction of the location of laminar-turbulent transition is a key factor in defining the dimensions and materials used for the thermal protection system (TPS). Yet, the fundamental physical processes related to the laminar-turbulent transition in high-speed boundary layers are not well understood. This is true even at the first stage of the process, that is, amplification of small linear perturbations. Due to small amplification rates, this first stage can take place for a long downstream distance. For that reason, it is important to develop a numerical method able to compute this stage accurately and thus predict transition correctly.

Unlike incompressible flows, high-speed boundary layers can possess more than one instability mode. These modes usually correspond to separate frequency bands in a stability diagram. The first mode is similar to the incompressible instability, a difference being that often first-mode oblique waves are more amplified than 2-D disturbances. Mack (1969) investigated the linear instability of high-speed boundary layer theoretically, in particular with respect to second and higher mode disturbances.

At a low temperature, a gas usually behaves as a calorically perfect gas. In high-speed flows, the temperature inside the boundary layer might be very high and, as a result, the gas properties such as specific heat become a function of temperature (thermally perfect gas). At even higher temperatures, chemical reaction processes occur and change the composition of the gas. If the flow velocity is small compared to chemical reaction rates, the gas will be in a state of chemical equilibrium. For higher speeds or smaller reaction rates, non-equilibrium effects may occur.

The aim of the present study is to first verify an existing numerical method in computing amplification of small-amplitude disturbances. Second, this numerical method is extended to handle different gas models. Third, we want to study the qualitative influence of high-temperature gas effects on boundary-layer stability, under the conditions of chemical equilibrium.

2. Governing equations

The governing equations are the time-dependent 3-D Navier-Stokes equations for a compressible fluid in non-dimensional form. These equations are formulated for a mixture of perfect gases, where chemical reactions can take place with an infinite reaction rate (so-called chemical equilibrium). Non-dimensionalization is based on the freestream conditions: temperature $\tilde{T}_\infty$, density $\tilde{\rho}_\infty$, specific heat ratio $\gamma_\infty = \tilde{c}_{p,\infty}/\tilde{c}_{v,\infty}$, a reference

length $\tilde{L}_{ref}$, and the speed of sound $\tilde{c}_\infty$ (all dimensional quantities are marked by $\tilde{\cdot}$):

$$\rho = \frac{\tilde{\rho}}{\tilde{\rho}_\infty}, \quad u_i = \frac{\tilde{u}_i}{\tilde{c}_\infty}, \quad E = \frac{\tilde{E}}{\tilde{\rho}_\infty \tilde{c}_\infty^2}, \quad p = \frac{\tilde{p}}{\tilde{\rho}_\infty \tilde{c}_\infty^2}, \quad T = \frac{\tilde{T}}{(\gamma_\infty - 1)\tilde{T}_\infty}, \tag{2.1}$$

$$x_i = \frac{\tilde{x}_i}{\tilde{L}_{ref}}, \quad t = \frac{\tilde{t} \cdot \tilde{c}_\infty}{\tilde{L}_{ref}}\,. \tag{2.2}$$

This results in the following set of equations for mass, momentum and energy conservation:

$$\frac{\partial \rho}{\partial t} + \frac{\partial}{\partial x_j}\left(\rho u_j\right) = 0, \tag{2.3}$$

$$\frac{\partial \rho u_i}{\partial t} + \frac{\partial}{\partial x_j}\left(\rho u_i u_j + p\delta_{ij}\right) = \frac{\partial \sigma_{ij}}{\partial x_j}, \qquad i = 1, 2, 3, \tag{2.4}$$

$$\frac{\partial E}{\partial t} + \frac{\partial}{\partial x_j}\left[\left(E + p\right) u_j\right] = -\frac{\partial q_{ij}}{\partial x_j} + \frac{\partial}{\partial x_k}\left(u_j \sigma_{ij}\right)\,. \tag{2.5}$$

In these equations, the absolute energy E, the viscous stress tensor σ_{ij} and the heat flux vector q_j are defined as:

$$E = e\rho + \frac{1}{2}\rho u_i u_i, \tag{2.6}$$

$$\sigma_{ij} = \frac{\mu}{Re}\left(\frac{\partial u_i}{\partial x_j} + \frac{\partial u_j}{\partial x_i} - \frac{2}{3}\frac{\partial u_k}{\partial x_k}\delta_{ij}\right), \tag{2.7}$$

$$q_j = q_j^T + q_j^p = -\frac{1}{Re_\infty Pr_\infty Ec_\infty} \cdot k_e \frac{\partial T}{\partial x_j} - \frac{1}{Re_\infty} \cdot b_e \frac{1}{\rho}\frac{\partial p}{\partial x_j}\,. \tag{2.8}$$

The coefficients k_e and b_e in Eq. (2.8) are defined as:

$$k_e = \frac{\tilde{k}_e}{\tilde{k}_\infty} = \frac{\tilde{k}_f}{\tilde{k}_\infty} + \frac{\tilde{\rho}}{\tilde{k}_\infty}\,\frac{\partial}{\partial \tilde{T}}\left(\sum_s \tilde{\rho}_s \tilde{U}_s \tilde{h}_s\right)\Bigg|_{\tilde{p}}, \tag{2.9}$$

$$b_e = \frac{\tilde{b}_e}{\mu_\infty} = \frac{\tilde{\rho}^2}{\tilde{\mu}_\infty}\,\frac{\partial}{\partial \tilde{p}}\left(\sum_s \tilde{\rho}_s \tilde{U}_s \tilde{h}_s\right)\Bigg|_{\tilde{T}}\,. \tag{2.10}$$

Here, $\tilde{k}_f$ is the thermal conductivity of a frozen gas mixture, which is a mixture whose composition does not change as a result of chemical reactions. $\tilde{U}_s$, $\tilde{\rho}_s$, $\tilde{h}_s$ denote diffusion velocity, density, and enthalpy of the species s, respectively.

2.1. *Dimensionless parameters*

The appropriate dimensionless parameters are the Reynolds number Re_∞, Prandtl number Pr_∞, and Eckert number Ec_∞:

$$Re_\infty = \frac{\tilde{\rho}_\infty \tilde{c}_\infty \tilde{L}_{ref}}{\tilde{\mu}_\infty} = Re^* \cdot \frac{1}{M_\infty}, \tag{2.11}$$

$$Pr_\infty = \frac{\tilde{\mu}_\infty \tilde{c}_{p,\infty}}{\tilde{k}_\infty}, \tag{2.12}$$

$$Ec_\infty = \frac{\tilde{c}_\infty^2}{\tilde{c}_{p,\infty}\left(\gamma_\infty - 1\right)\tilde{T}_\infty} = Ec^* \cdot \frac{1}{\left(\gamma_\infty - 1\right) M_\infty^2}\,. \tag{2.13}$$

The superscript * denotes quantities as they are commonly used in the literature.

These require a Mach number M_∞, which is defined as:

$$M_\infty = \frac{\tilde{u}_\infty}{\tilde{c}_\infty}\,. \tag{2.14}$$

2.2. *Equation of State*

To close the system of equations, an equation of state is needed for the gas mixture. In the present case, its non-dimensional form is:

$$p = \frac{R}{Ec_\infty} \cdot \rho T\,. \tag{2.15}$$

In this equation, $R{=}\tilde{R}/\tilde{c}_{p,\infty}$ is the gas constant of the mixture.

3. High-temperature gas models

We will consider three different types of gases: a calorically perfect gas, a thermally perfect gas, and a mixture of chemically reacting gases in equilibrium (infinitely large reaction rates). These types will be detailed in the following sections, including more than one problem formulation for each gas type.

3.1. *Calorically perfect gas*

For a calorically perfect gas, the specific heat c_p and the transport properties k_e and μ are constant. The internal enthalpy $h{=}c_pT$ $(=\sum h_s)$ is only a function of temperature and the gas composition does not change. As a result, the internal energy $e{=}h - p/\rho$ in Eq. (2.6) is given by:

$$e = \frac{1}{\gamma_\infty - 1}\,\frac{p}{\rho}\,. \tag{3.1}$$

The coefficients in the definition of the heat-flux vector Eq. (2.8) are:

$$k_e = \mu, \quad b_e = 0\,. \tag{3.2}$$

Due to the fact that for a calorically perfect gas, the speed of sound is defined as $\tilde{c}^2_\infty{=}\gamma_\infty\tilde{R}\tilde{T}_\infty$, we have $Ec^*{=}(\gamma_\infty - 1)\,M^2_\infty$ and hence:

$$Ec_\infty = 1\,. \tag{3.3}$$

Note that Eq. (3.3) holds in case of a thermally perfect gas, too, or even in case of chemical reactions, if a calorically / thermally perfect gas exists in the freestream. This will be indeed true for all cases investigated here.

The non-dimensional viscosity is computed from Sutherland's law:

$$\mu = T^{3/2} \cdot \frac{1 + \tilde{T}_S/\tilde{T}_\infty}{T + \tilde{T}_S/\tilde{T}_\infty}, \quad \text{with } \tilde{T}_s = 110.4K\,. \tag{3.4}$$

Another formulation arises if we compute the viscosity from a simple linear law:

$$\mu = T\,. \tag{3.5}$$

For a calorically perfect gas, the gas constant is given by:

$$R = \frac{\gamma_\infty - 1}{\gamma_\infty}\,. \tag{3.6}$$

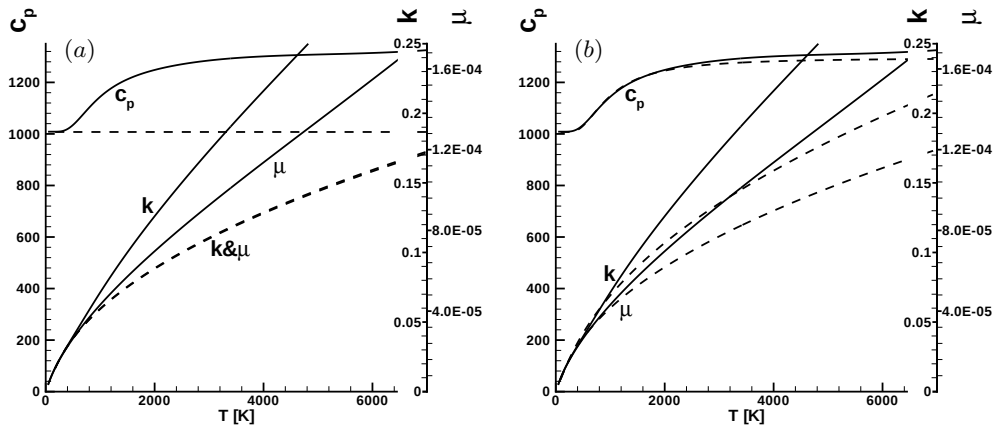

FIGURE 1. Gas properties $\tilde{c}_p[J/K]$, $\tilde{k}[W/m\,K]$, $\tilde{\mu}[kg/m\,sec]$ for different gas models for air. (a) calorically perfect gas (dashed) vs. thermally perfect gas according to § 3.2.1 (solid). (b) thermally perfect gas, model according to § 3.2.1 (solid) vs. model according to § 3.2.2 (dashed).

3.2. *Thermally perfect gas*

In a thermally perfect gas, the internal energy for a molecule is the sum of translational, rotational, and vibrational energy. While the former two contributions are proportional to the temperature, the latter one has a more complicated temperature dependence.

Still, the internal energy is only a function of temperature. It can be computed based on the internal enthalpy h or based on a non-constant $c_p{=}\tilde{c}_p(T\cdot\tilde{T}_\infty)/\tilde{c}_{p,\infty}$ as:

$$e(T) = h - p/\rho = h_0 + \int_{T_0}^{T} c_p dT - p/\rho \quad \text{with} \quad h_0 = c_p(T_0)\cdot T_0\,. \tag{3.7}$$

The gas composition does not change, and hence:

$$k_e = \frac{\tilde{k}_f(T\cdot\tilde{T}_\infty)}{\tilde{k}_\infty}, \quad b_e = 0\,. \tag{3.8}$$

As previously indicated, Eq. (3.3) is still valid. Moreover, due to the fact that the gas composition does not change, the gas constant R does not change and Eq. (3.6) still holds.

So far, we have assumed that we know the functions $\tilde{c}_p(T{\cdot}\tilde{T}_\infty)$ and $\tilde{c}_{p,\infty}{=}\tilde{c}_p(\tilde{T}_\infty)$ as well as a law for the frozen thermal diffusion $\tilde{k}_f{=}\tilde{k}_f(T\cdot\tilde{T}_\infty)$ and $\tilde{k}_\infty{=}\tilde{k}_f(\tilde{T}_\infty)$. Moreover, the viscosity $\tilde{\mu}{=}\tilde{\mu}(T\cdot\tilde{T}_\infty)$ dependence and $\tilde{\mu}_\infty{=}\tilde{\mu}(\tilde{T}_\infty)$ are known. In the next two sections, these functions will be discussed.

3.2.1. *Barbante & Magin (2004)'s frozen gas*

Gas properties are computed based on a kinetic theory approach (for details see Barbante & Magin 2004). The resulting gas properties are given in Fig. 1(a), where they are compared to a calorically perfect gas.

3.2.2. *Malik & Anderson (1991)'s imperfect gas*

This model is based on equations given in Malik & Anderson (1991). The specific heat $\tilde{c}_p$ is defined as:

$$\tilde{c}_p = \tilde{c}_{p,\infty} \left\{ 1 + \frac{\gamma_\infty - 1}{\gamma_\infty} \left[\left(\frac{\tilde{\Theta}}{\tilde{T}} \right)^2 \frac{e^{\tilde{\Theta}/\tilde{T}}}{(e^{\tilde{\Theta}/\tilde{T}} - 1)^2} \right] \right\} \quad \text{with} \quad \tilde{\Theta} = 3055\,K\,. \tag{3.9}$$

As noted by Malik & Anderson (1991) Eq. (3.9) is valid only up to $\tilde{T}$=2500K. For that reason, results obtained with this model are believed to be less accurate than those from Barbante & Magin (2004)'s frozen gas model. Thermal conductivity $\tilde{k}_e$ is computed from:

$$\tilde{k}_e = d_3 \frac{\tilde{T}^{0.5}}{1 + (d_4/\tilde{T}) 10^{-d_5/\tilde{T}}}, \tag{3.10}$$
$$\text{with} \quad d_3 = 2.646 \cdot 10^{-3}\,W/m\,K, d_4 = 245.4\,K, d_5 = 12\,K\,.$$

Viscosity $\tilde{\mu}$ is computed from Sutherland's law, however with slightly different values compared to Eq. (3.4):

$$\tilde{\mu} = d_1 \frac{\tilde{T}^{0.5}}{1 + (d_2/\tilde{T})}, \tag{3.11}$$
$$\text{with} \quad d_1 = 1.458 \cdot 10^{-6}\,kg/m\,sec, d_2 = 110.4\,K\,.$$

In Fig. 1(b), the resulting gas properties are compared with those obtained with the model by Barbante & Magin (2004).

3.3. *Chemically reacting gas in equilibrium*

In a chemically reacting gas in equilibrium, the chemical reaction rates are infinite so that the gas composition as well as gas properties are solely a function of temperature and pressure (or density). The gas is assumed to be a mixture of thermally perfect gases, while the exact composition is determined by chemical equilibrium.

The internal energy e is the sum of contributions from all species s:

$$e = \frac{\tilde{e}}{Ec_\infty \tilde{c}_{p,\infty}(\gamma_\infty - 1)\tilde{T}_\infty \tilde{\rho}_\infty} = -\frac{p}{\rho} + \sum_s h_s\,. \tag{3.12}$$

In this equation, h_s contains the heat of formation for species s, respectively.

The coefficients in the definition of the heat-flux vector and the viscosity are known functions of both temperature and pressure:

$$k_e = \frac{\tilde{k}_e(T \cdot \tilde{T}_\infty, \tilde{p})}{\tilde{k}_\infty}, \quad b_e = \frac{\tilde{b}_e(T \cdot \tilde{T}_\infty, \tilde{p})}{\tilde{\mu}_\infty}, \quad \mu = \frac{\tilde{\mu}(T \cdot \tilde{T}_\infty, \tilde{p})}{\tilde{\mu}_\infty}\,. \tag{3.13}$$

In contrast to a calorically or thermally perfect gas, R is no longer a constant, but dependent on temperature and pressure:

$$R = \frac{\tilde{R}(T \cdot \tilde{T}_\infty, \tilde{p})}{\tilde{c}_{p,\infty}}\,. \tag{3.14}$$

3.3.1. *Barbante & Magin (2004)'s chemically reacting gas in equilibrium*

Again, gas properties and also gas composition are computed based on the approach by Barbante & Magin (2004). As a gas, we use air composed of the five species O_2, N_2, NO,

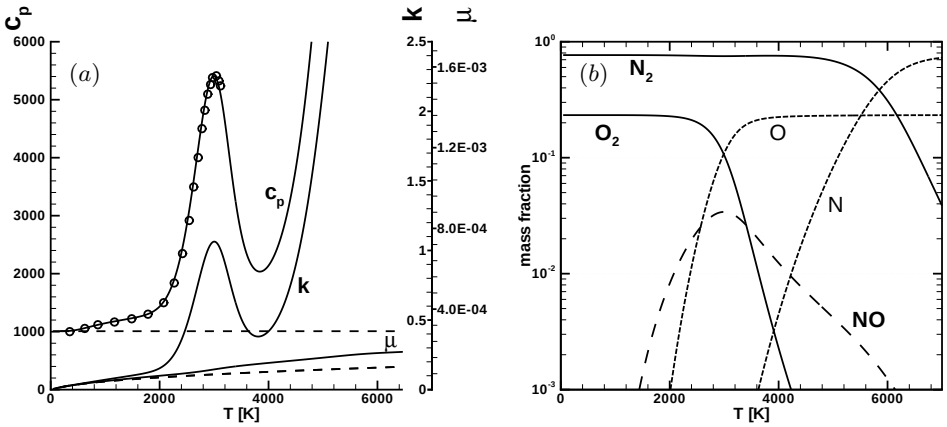

FIGURE 2. (a) Gas properties $\tilde{c}_p[J/K]$, $\tilde{k}[W/m\,K]$, $\tilde{\mu}[kg/m\,sec]$ for air at $\tilde{p}$=3596Pa, calorically perfect gas (dashed lines) vs. chemically reacting gas in equilibrium, model according to § 3.3.1 (solid lines), together with c_p derived from Figs. 1b and 2a of Malik & Anderson (1991) (open symbols). (b) Gas composition for a chemically reacting gas in equilibrium, model according to § 3.3.1.

O, and N. The resulting gas properties are given in Fig. 2(a) in comparison to a calorically perfect gas. The strong variation in $\tilde{c}_p$ and $\tilde{k}_e$ is due to chemical reactions, which can be seen from a comparison of gas properties (Fig. 2a) and gas composition (Fig. 2b). Around the temperature where dissociation of O_2 into O takes place ($\tilde{T} \approx 3500\,K$), and again where dissociation of N_2 into N occurs ($\tilde{T} \approx 7000\,K$), $\tilde{c}_p$ and $\tilde{k}_e$ reach peak values.

3.3.2. *Barbante & Magin (2004)'s chemically reacting gas in equilibrium (simplified)*

In this simplified model, we neglect the pressure dependence of all gas quantities. The result is:

$$k_e = \frac{\tilde{k}_e(T \cdot \tilde{T}_\infty)}{\tilde{k}_\infty}, \quad b_e = 0, \quad \mu = \frac{\tilde{\mu}(T \cdot \tilde{T}_\infty)}{\tilde{\mu}_\infty}, \quad R = \frac{\tilde{R}(T \cdot \tilde{T}_\infty)}{\tilde{c}_{p,\infty}}\,. \tag{3.15}$$

This approach is believed to be reasonably accurate in boundary-layer type flows, where the pressure variation is small.

4. Numerical method

The basis for the numerical method applied here is a code developed by Nagarajan *et al.* (2007). It was extended in order to handle different gas models. In the case of a calorically perfect gas, the original version of the code was used.

In a pre-processing step, all gas properties are computed as a function of internal energy $\tilde{e}$. The non-dimensional internal energy is obtained from E as:

$$e = (E - \frac{1}{2}\rho u_k u_k)/\rho\,. \tag{4.1}$$

With a known e, the dimensional internal energy $\tilde{e}$ can be computed based on Eq. (3.12). This quantity is used to look-up the dimensional temperature $\tilde{T}$, viscosity $\tilde{\mu}$, thermal conductivity $\tilde{k}_e$, and gas constant $\tilde{R}$, which are all subsequently non-dimensionalized. The look-up procedure is based on a fourth-order Lagrange interpolation.

case	Re^*	Pr_∞	Ec_∞	M_∞	$\tilde{T}_\infty$	reference
1	10^5	0.71	1	4.8	55.4K	Pagella *et al.* (2002)
2	10^5	0.7	1	10.0	350.0K	Malik & Anderson (1991)

TABLE 1. Overview of simulation parameters for two different cases. Pr_∞ is used only for a calorically perfect gas.

case	x_0	x_1	y_0	y_1	z_0	z_1	NMAX	MMAX	KMAX
1	1.6065	30.1665	0	1.575	-0.604	0.604	800	200	(10)
2	11.6065	68.7265	0	1.575	-	-	1600	200	-

TABLE 2. Overview of domain sizes and resolution for the two different cases.

4.1. *Discretization, integration domains and boundary conditions*

Two different test cases will be considered. Parameters of these cases are given in Table 1. If a non-calorically-perfect gas is used, the Pr_∞ given in the table is replaced by the corresponding value for the respective gas model and freestream temperature.

The grid is uniformly spaced in streamwise direction x ($NMAX$ points) and spanwise direction z ($KMAX$ points, for 3-D calculations only). In wall-normal direction, a grid stretching is applied according to the following formula, with κ=0.15 and m=1 ... $MMAX$:

$$y_m = y_{max}\left((1-\kappa)\left(\frac{m-1}{MMAX-1}\right)^3 + \kappa\frac{m-1}{MMAX-1}\right). \tag{4.2}$$

The sizes of the integration domains and the number of grid points used are given in Table 2. The streamwise resolution corresponds approximately to 16 grid points per streamwise wavelength of the instability wave in case 1 (2-D) and to 48 grid points per streamwise wavelength in case 2.

At the inflow x_0, a self-similar solution is prescribed while the wall (at y=0) is adiabatic with a no-penetration and no-slip condition. At the outflow x_1 and in the freestream y_1, the solution is damped towards a laminar state (a uniform flow in the freestream with $u(y_1)$=M_∞ and a self-similar solution at the outflow) with the aid of a forcing term added to the equations (sponge region). In the 3-D case, the flow is periodic in spanwise direction. To visualize the streamwise axis, a local Reynolds number Re_x=R_x=$\sqrt{x \cdot Re^*}$ will be used below in place of x.

In the test cases, a small-amplitude disturbance is forced via blowing and suction at the wall (subscript $_w$) in a way suggested by Pagella *et al.* (2002):

$$(\rho v)_w = A_v \cdot \sin(\omega t) \cdot cos(\beta z) \cdot \sin(n_c \xi) \cdot e^{-\xi^2/\sqrt{2}}, \tag{4.3}$$

$$\xi = (x - x_{strip,0})/x_{strip,L}\,. \tag{4.4}$$

Forcing parameters for the different cases are given in Table 3. These values were chosen for best matching with the reference in the first case, and then adapted slightly for the second case to trigger the instability wave as good as possible. The non-dimensional forcing frequency is defined as ω=$F \cdot M_\infty \cdot Re^*$, while the spanwise wave number corresponds to β=$2\pi/(z_1 - z_0)$.

case	n_c	$x_{strip,0}$	$x_{strip,L}$	ω	β	A_v	$Re_{x_{strip,0}}$
1 (2-D)	16	5.49	4.203	48	0	$2 \cdot 10^{-4}$	741
1 (3-D)	16	5.49	4.203	48	5.2	$2 \cdot 10^{-4}$	741
2 (2-D)	4.706	15.49	4.203	34	0	$2 \cdot 10^{-4}$	1245

TABLE 3. Overview of the forcing parameters for the two different cases.

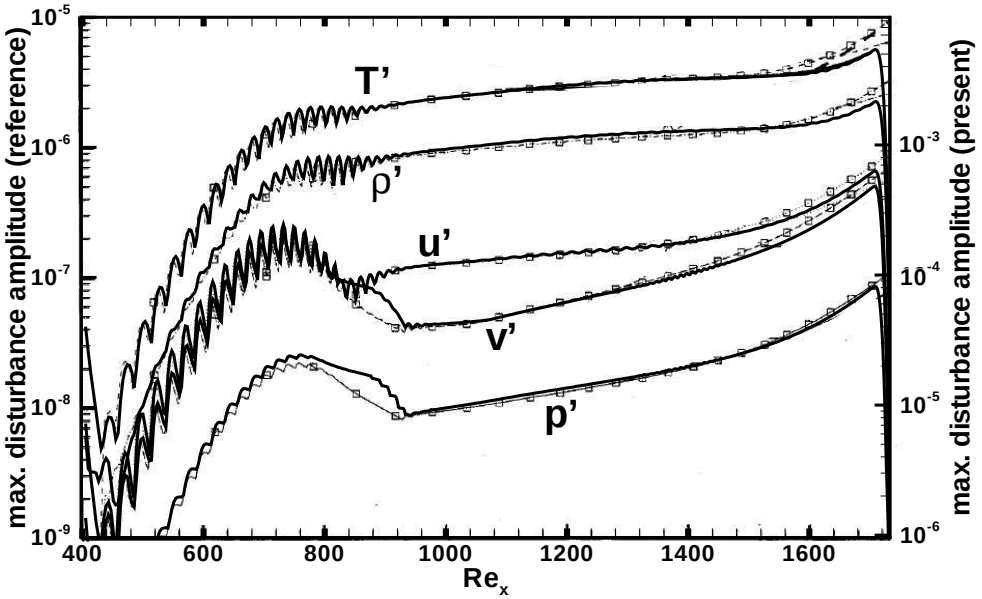

FIGURE 3. Maximum disturbance amplitudes of different flow variables from present calculation (solid lines) compared with Pagella *et al.* (2002) (lines with symbols). Two-dimensional disturbance with frequency F=10^{-4}, the viscosity is computed from Sutherland's law Eq. (3.4).

4.2. *Verification*

To ensure that the code is able to accurately simulate the evolution of small-amplitude disturbances, case 1 was selected for which numerical results are published in Pagella *et al.* (2002) for a calorically perfect gas.

The computation is advanced up to 96 forcing periods and then Fourier analyzed in time with the forcing frequency as the fundamental frequency. For the 2-D disturbance, we observe a very close match with respect to the amplification (Fig. 3), wall-normal amplitude functions (Fig. 4), and phase functions (Fig. 5). Close agreement is observed also for the 3-D / oblique disturbance (Fig. 6, Fourier transformed also in span).

Only very far downstream do we observe a deviation in amplification towards lower disturbance growth (Fig. 3). An additional calculation shows that this is due to the viscosity law used. In the reference, a blending between a linear law and Sutherland's law is used, while we use a single law for the entire temperature range. If we use a linear law instead, we see a deviation towards stronger disturbance growth (Fig. 7).

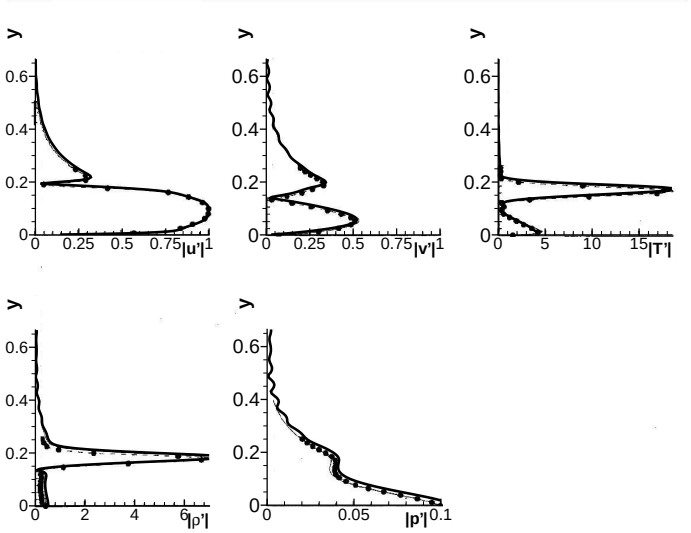

FIGURE 4. Amplitude distributions at Re_x=1330: present results (thick lines) compared with reference numerical results (thin lines) and linear stability theory (symbols), both taken from Pagella *et al.* (2002). The disturbance frequency is F=10^{-4}.

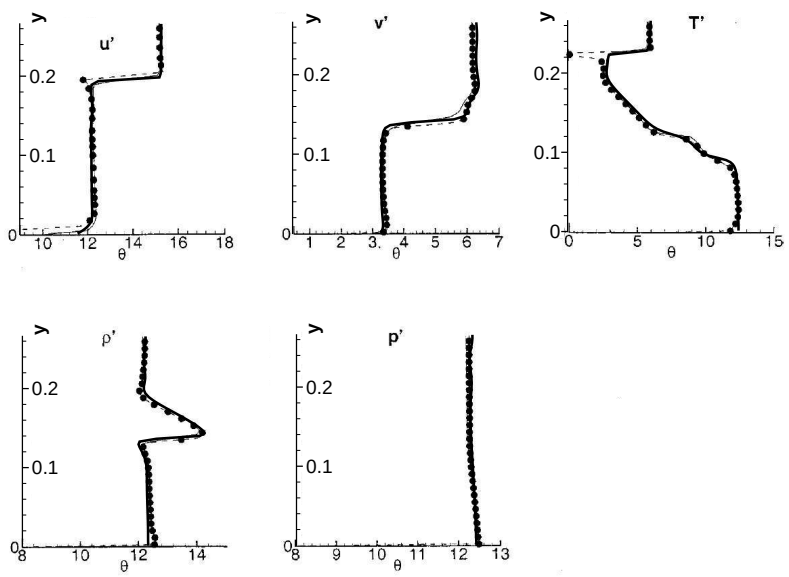

FIGURE 5. Phase distributions at Re_x=1330: present results (thick lines) compared with reference numerical results (thin lines) and linear stability theory (symbols), both taken from Pagella *et al.* (2002). The disturbance frequency is F=10^{-4}.

Based on the good agreement observed, we conclude that the present method is well suited to investigate the amplification of a small-amplitude disturbance.

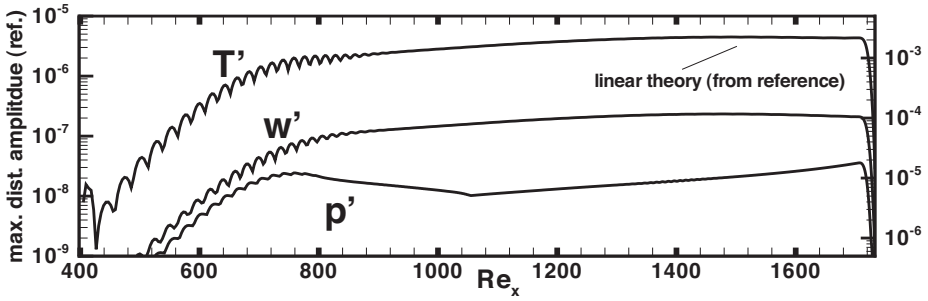

FIGURE 6. Maximum disturbance amplitudes of flow variables compared with Pagella *et al.* (2002). Oblique disturbances with frequency F=10^{-4} and spanwise wave number β=5.2, the viscosity is computed from Sutherland's law Eq. (3.4).

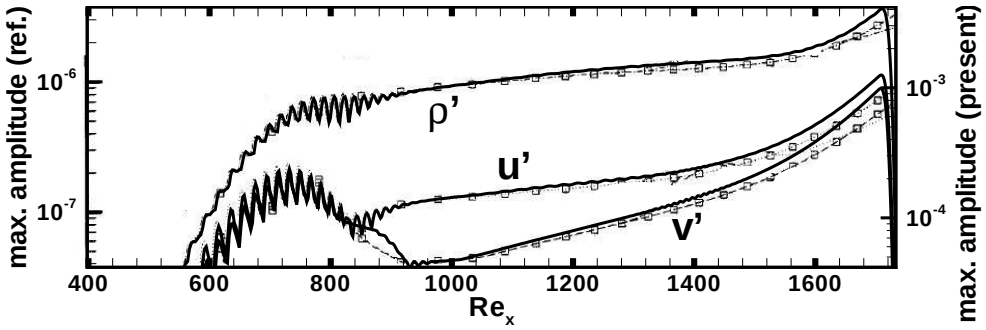

FIGURE 7. Maximum disturbance amplitudes of flow variables from present calculation (solid lines) compared with Pagella *et al.* (2002) (lines with symbols). Two-dimensional disturbance with frequency F=10^{-4}, the non-dimensional viscosity is equal to the non-dimensional temperature (linear law) as in Eq. (3.5).

5. High-temperature gas effects on linear instability in a boundary layer

The problem formulation for this case (case 2 in Table 1) is guided by investigations of Malik & Anderson (1991). They investigate the linear instability of a boundary layer for a calorically perfect gas, a thermally perfect gas (according to § 3.2.2) and a chemically reacting gas in chemical equilibrium. However, the latter model used in that reference is different than the model described in § 3.3.1.

5.1. *Mean flow:* M_∞=10 *boundary layer*

The effect of chemical reactions on the mean flow is to reduce the thickness of the boundary layer (Fig. 8*a*) and to decrease the temperature at the wall (Fig. 8*b*). Due to the differences in gas model, no perfect match between the present results and the results of Malik & Anderson (1991) for the chemically reacting gas is obtained, nor should it be expected. Nevertheless, the results are quite similar. For the case of a thermally perfect gas (not shown), we observe a reduction in boundary-layer thickness only for Malik & Anderson (1991)'s model, while the temperature at the wall is reduced in both gas models.

The numerical simulation results were verified to match the self-similar profiles even inside the domain reasonably well.

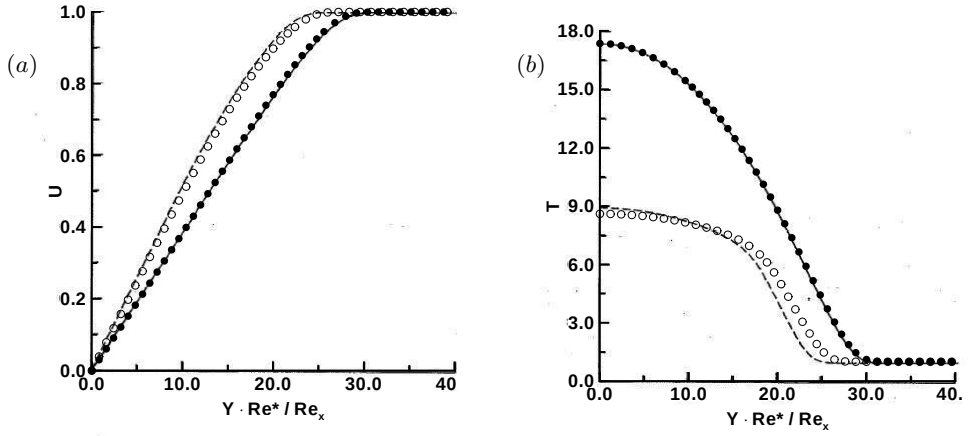

FIGURE 8. Self-similar laminar boundary-layer profiles, for a calorically perfect gas (solid lines and filled symbols) and a chemically reacting gas in equilibrium at $\tilde{T}_\infty$=350K, $\tilde{p}_\infty$=3596Pa (dashed lines and open symbols), present results (symbols) versus results from Malik & Anderson (1991) (lines). (a) streamwise velocity and (b) temperature.

5.2. *Disturbance amplification*

As in the previous case, we use blowing and suction at the wall according to Eq. (4.3) to introduce a single-frequency disturbance, forcing parameters are given in Table 3 (case 2). According to Malik & Anderson (1991), the present disturbance can be classified as a second-mode disturbance.

The computation is advanced up to 96 forcing periods and then Fourier analyzed in time with the forcing frequency as the fundamental frequency. The resulting amplification for a thermally perfect gas is shown in Fig. 9(a), together with the phase speed of the wave based on the wall pressure p_w (Fig. 9b), which is computed from:

$$c_{ph} = Re^* \cdot F \cdot \left(\frac{\partial \Phi(p_w)}{\partial x} \right)^{-1}. \tag{5.1}$$

Corresponding results for a chemically reacting gas can be found in Fig. 10.

From these figures, it is apparent that high-temperature gas effects have a strong impact on the evolution of small-amplitude disturbances. A certain, unique trend is not observable. Rather, high-temperature gas effects increase the amplification rate at one x position while they reduce it at another position.

For a calorically perfect gas, a good match with the linear stability results of Malik & Anderson (1991) is observed (Fig. 9). For the chemically reacting gas (Fig. 10), amplification rates agree well, too, while phase velocities are somewhat different. In light of the differences for the mean profiles observed in §5.1, a perfect match again cannot be expected. Nevertheless, the qualitative effect of chemical reactions at Re_x=2000 is the same: amplification is enhanced while the phase velocity is lowered.

6. Future work

For the case with M_∞=4.8, the influence of a localized roughness element on disturbance amplification will be studied. For the case with M_∞=10, the presented results will be supplemented by those for the complete model of a chemically reacting gas in

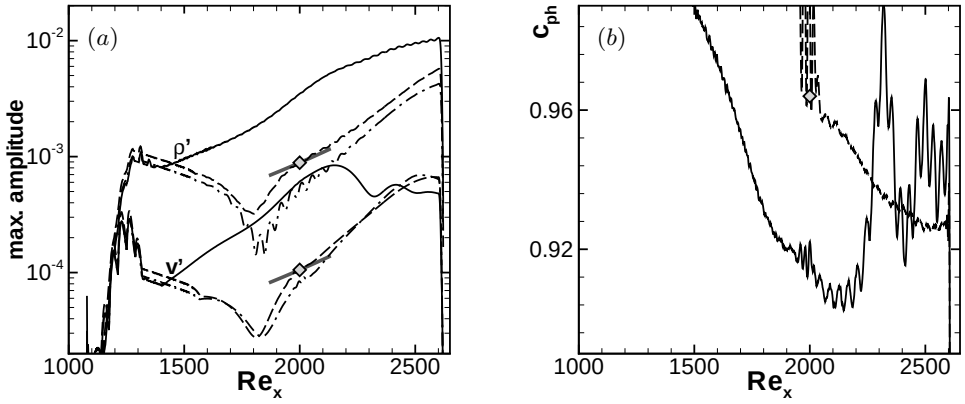

FIGURE 9. Streamwise disturbance evolution for a thermally perfect gas, model according to § 3.2.1 (solid) and model according to § 3.2.2 (dash-dotted), and a calorically perfect gas (dashed). Amplification rate and phase velocity from Malik & Anderson (1991) at Re_x=2000 are marked with a diamond symbol. (a) amplification and (b) phase velocity.

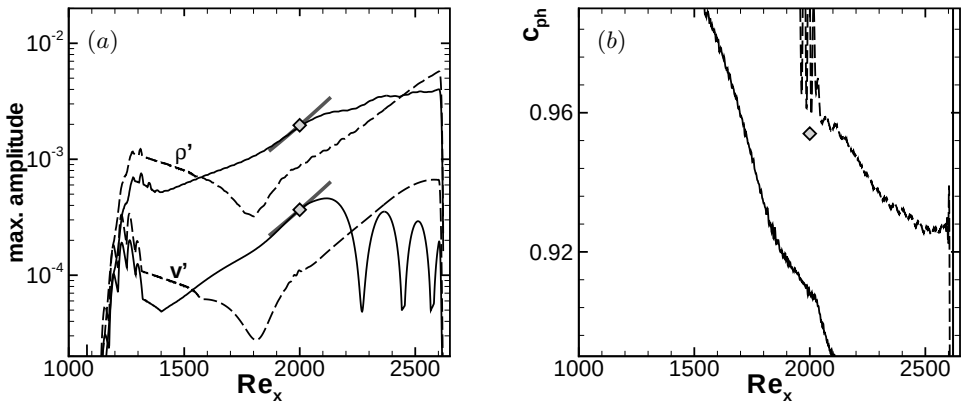

FIGURE 10. Streamwise disturbance evolution for a chemically reacting gas in equilibrium, simplified model, (solid) compared to a calorically perfect gas (dashed). Amplification rate and phase velocity from Malik & Anderson (1991) at Re_x=2000 are marked with a diamond symbol. (a) amplification and (b) phase velocity.

equilibrium as described in § 3.3.1. Moreover, an investigation of different frequencies that correspond to first mode and third mode disturbances is planned.

7. Acknowledgments

Financial support from the National Aeronautics and Space Administration (NASA) under award No. NNX07AC29A is gratefully acknowledged. The authors acknowledge the High Performance Computing Center at Stanford University for providing computing resources. We are grateful to S. Lele and A. Mani, Stanford University, for useful

discussions and for providing the simulation code, and to T. Magin for useful discussions and for providing the code to compute high-temperature gas properties.

REFERENCES

Barbante, P. F. & Magin, T. E. 2004 Fundamentals of hypersonic flight – Properties of high temperature gases. In *RTO AVT Lecture Series on "Critical Technologies for Hypersonic Vehicle Development," pp. 5.1–5.50*. van Karman Institut, Rhode-Saint-Genese, Belgium.

Mack, L. M. 1969 Boundary layer stability theory. *Tech. Rep.* JPL-900-277-REV-A; NASA-CR-131501. Jet Propulsion Laboratory, NASA.

Malik, M. R. & Anderson, E. C. 1991 Real gas effects on hypersonic boundary-layer stability. *Phys. Fluids A* **3** (5), 803–821.

Nagarajan, S., Lele, S. K. & Ferziger, J. H. 2007 Leading-edge effects in bypass transition. *J. Fluid Mech.* **572**, 471–504.

Pagella, A., Rist, U. & Wagner, S. 2002 Numerical investigations of small-amplitude disturbances in a boundary layer with impinging shock wave at Ma=4.8. *Phys. Fluids* **14** (7), 2088–2100.